# Photocatalytic Degradation of Methyl Violet and Auramine-O Dyes Using Ni/ZnO Nanocomposites for An Environmental Solution for Dye Wastewater

Ajmal Shah[1], Adnan[2], Talha Sharif[1], Muhammad Majid Khan[1], Zain ul Abidin[2], Muhammad Sohail[2], Farah Muhammad Zada[2], Naseer Khan[3], Fawad Ali[4*], Saba Zafar[5*]

## Abstract

Background: The increasing release of synthetic dyes, such as methyl violet (MV2B) and auramine O (AO), into water bodies from industrial effluents poses significant environmental and health risks due to their toxicity and persistence. Conventional wastewater treatment methods often fail to fully eliminate these dyes, leading to a demand for advanced techniques like photocatalysis. This study examines the efficacy of Ni-doped ZnO (Ni/ZnO) photocatalysts for the photodegradation of MV2B and AO dyes under UV irradiation. Methods: Ni/ZnO catalysts were synthesized via wet impregnation, followed by calcination and characterization through SEM, EDX, and XRD to confirm morphology, elemental composition, and structural changes. Photodegradation experiments were conducted with various dye concentrations, catalyst dosages, and irradiation times under controlled pH. The removal efficiency was assessed by measuring absorption changes pre- and post-degradation. Results: The optimized conditions showed significant degradation efficiencies of 86.36% and 69.31% for MV2B and AO, respectively. The study revealed that increasing catalyst dosage enhanced degradation by providing more active sites, while degradation efficiency decreased at higher dye concentrations due to competition for these sites. Kinetic analysis demonstrated that MV2B degradation followed a pseudo-second-order model, whereas AO conformed to a pseudo-first-order kinetic model. Conclusion: The Ni/ZnO photocatalyst proved highly effective in degrading MV2B and AO dyes, with pH optimization further improving performance. This research supports Ni/ZnO photocatalysis as a promising approach for treating dye-contaminated wastewater, contributing to sustainable environmental remediation efforts.

**Keywords:** Dye pollution, photocatalysis, Ni/ZnO, methyl violet, Auramine-O

***Significance*** | This study demonstrated Ni/ZnO photocatalysts as efficient, sustainable agents for degrading toxic dyes in wastewater, minimizing environmental impacts.

*Correspondence. Fawad Ali, Institute of Biotechnology and Microbiology, Bacha Khan University Charsadda, Pakistan. E-mail: fawadansi@gmail.com
Saba Zafar, Changchun University of Science and technology Changchun, R.P. China.
E-mail: szbutt11@gmail.com

Editor Muhit Rana, Ph.D., And accepted by the Editorial Board July 18, 2024 (received for review July 18, 2024)

## Introduction

The widespread use of synthetic dyes in various industrial applications, including cosmetics, food processing, pharmaceuticals, paper and pulp production, textiles, leather treatment, and printing, has led to significant environmental and health concerns (Qamar et al., 2021; Mosleh et al., 2016; Shojaei et al., 2021). Despite their diverse applications, an estimated 10-15% of synthetic dyes produced annually are lost to wastewater during the manufacturing process of colored goods (Bouasla, Samar, &

**Author Affiliation.**
[1] Department of Chemistry, Abdul Wali Khan University, Mardan, Khyber Pakhtunkhwa, Pakistan.
[2] Institute of Chemical Sciences, University of Swat, Swat, Khyber Pakhtunkhwa, Pakistan.
[3] Nutrition Division Institute of Health Islamabad, Pakistan.
[4] Institute of Biotechnology and Microbiology, Bacha Khan University Charsadda, Pakistan.
[5] Changchun University of Science and technology Changchun, R.P. China.

**Please Cite This:**
Adnan, Ajmal Shah, Talha Sharif, Muhammad Mjid Khan, Zain ul Abidin, Muhammad Sohail, Farah Muhammad Zada, Naseer Khan, Fawad Ali, Saba Zafar (2024). "Photocatalytic Degradation of Methyl Violet and Auramine-O Dyes Using Ni/ZnO Nanocomposites for An Environmental Solution for Dye Wastewater", Biosensors and Nanotheranostics, 3(1),1-8,9940.

Ismail, 2010). This dye-laden wastewater presents a major challenge to environmental safety due to the toxic and often persistent nature of many synthetic dyes.

Currently, over 100,000 different commercial dyes are with an annual global production exceeding 700,000 tons (Adegoke & Bello, 2015; Zada et al., 2022). The demand for dyes in textile, cosmetic, and paper industries has escalated, leading to increased quantities of wastewater generated, particularly in countries like Pakistan where textile production is a key economic activity (Shah et al., 2018). Polluted wastewater from these industries is frequently discharged into freshwater bodies, introducing a range of hazardous organic pollutants, including dyes and other contaminants, which contribute to environmental degradation (Arunagiri, 2021; Humayun et al., 2016; Senthil Kumar & Arunagiri, 2021). This dye pollution has profound effects on aquatic ecosystems and also poses risks to terrestrial life, including humans, plants, and animals, through bioaccumulation and biomagnification.

Different classes of dyes have varying toxicological profiles depending on their chemical structures, stability, and persistence in the environment. Many dyes are particularly resilient to degradation, thus prolonging their environmental impact (Nazir et al., 2020; Naz et al., 2021). Exposure to toxic dyes can lead to numerous health issues, such as respiratory problems, liver and kidney damage, skin irritation, and even cancer (Naz et al., 2021). For instance, methyl violet 2B (MV2B), a commonly used aromatic azo dye with the chemical formula $C_{24}H_{28}ClN_3$, is widely utilized in textile and printing industries (Guzmán-Vargas et al., 2016). While MV2B is soluble in water, it is known to cause eye and respiratory irritation and has a reported LC-50 level of 0.047 mg/L for the freshwater fish Pimephales promelas, indicating significant toxicity at low concentrations (Sinha et al., 2014). Human exposure to MV2B has been linked to adverse health effects on the kidneys, liver, brain, and central nervous system, and it has also been shown to impede bacterial growth and the photosynthesis of aquatic plants (Humayun et al., 2016; Xu et al., 2019).

Auramine O (AO) is another highly toxic dye, characterized as a water-soluble cationic fluorescent dye. Its yellow hue makes it popular in the paper, textile, and dyeing industries, as well as in the treatment of leather and fisheries (Zhang et al., 1997; Zhu et al., 2015). AO is particularly hazardous due to its stability and persistence in the environment, leading to adverse effects on human health, including respiratory and nervous system damage, and allergic reactions. AO exposure is associated with risks of carcinogenicity and allergic reactions and is thus banned as a hazardous dye for use in food and medicine (Hmani et al., 2012; Qi et al., 2020). Furthermore, AO's environmental persistence reduces water transparency, thereby inhibiting photosynthesis and primary production in aquatic ecosystems (Ghaedi et al., 2015).

Given the substantial environmental and health risks posed by dyes, it is crucial to treat dye-contaminated industrial effluents before discharge. Conventional dye removal methods, such as physical adsorption, chemical coagulation, and biological treatments, often fall short due to the complex chemical structures and stability of many dyes (Qi et al., 2020; Kashif et al., 2024). Advanced techniques, including photocatalytic degradation, electrochemical methods, and ozonation, have emerged as promising approaches. For instance, photo-degradation processes using catalysts such as titanium dioxide ($TiO_2$) and zinc oxide (ZnO) have gained traction due to their ability to decompose dyes under UV light, ultimately mineralizing these pollutants into non-toxic by-products (Zada et al., 2022; Zaman et al., 2024). Such methods leverage catalysts' surface properties—density, porosity, and surface area—to enhance radical generation and achieve effective dye degradation.

Our research group has explored various catalysts for dye degradation, focusing on enhancing efficiency through modifications such as co-doping and nanostructuring. Recent catalysts investigated include $Pd/HAP/Fe_3O_4$, (Al, Ni)-co-doped ZnO, and Cu-ZnO photocatalysts. These materials were characterized through SEM, EDX, XRD, FTIR, XPS, and UV-vis spectroscopic techniques, providing insights into their structural and functional properties (Safavi & Momeni, 2012; Reddy et al., 2020). Specifically, $TiO_2$ and UV light were successfully used for the degradation of methyl violet, and Ni-$TiO_2$/ACFs composite catalysts exhibited enhanced activity under microwave induction for the degradation of methyl violet in water (Sun et al., 2020). Additionally, Cu-Fe layered double hydroxides (LDH) have shown promise in sulfate radical-mediated degradation of dyes (Ma et al., 2018).

This study investigated the use of Ni/ZnO photocatalysts, leveraging their unique properties for the photodegradation of dyes under near-UV or solar light. ZnO is favored in environmental applications due to its high UV absorption, affordability, non-toxicity, and photostability (SivaKarthik et al., 2017; Zhang et al., 2012). Furthermore, the presence of Ni enhances ZnO's desulfurization performance, particularly with smaller particle sizes, resulting in improved dye adsorption and degradation capabilities (Zhang et al., 2012; Xu et al., 2016). ZnO nanoparticles hold significant potential for applications in transparent conductive coatings, photoanodes in dye-sensitized solar cells, and environmental pollutant degradation. While Ni-doped ZnO samples have lower band gap energies, their photocatalytic performance is affected by defects introduced by Ni, warranting further investigation to optimize activity and stability (Xu et al., 2016).

The persistent environmental and health impacts of industrial dye pollution necessitate effective and sustainable treatment solutions. Advances in photocatalysis and the development of novel materials such as Ni/ZnO hold promise for the efficient degradation of dyes, providing a pathway towards mitigating the ecological footprint of industrial effluents.

## 2.Materials and Methods

### *2.1. Reagent and chemicals*

Methyl violet 2B (MV2B), zinc oxide (ZnO) and nickel nitrate ($NiNO_3$), disodium hydrogen phosphate ($Na_2HPO_4$), potassium iodide (KI) were purchased from Sigma–Aldrich, citric acid (**$C_6H_8O_7$**), hydrogen peroxide ($H_2O_2$). All the chemicals were of high purity and were used as such.

### *2.2. Preparation of Ni/ZnO catalyst*

The catalyst was prepared by modified wet incipient impregnation method. About 10 g of ZnO catalyst was added to considerable amount of distilled water in a beaker, this was named solution A. About 5% $NiNO_3$ solution wasprepared in another beaker, which was termed as solution B. Solution A was poured into solution B and mixed well. After mixing the mixture of $NiNO_3$ solution and ZnO slurry was kept at room temperature until the dryness of the sample. Then the material was kept in an oven for 1 hour at 120 ºC. The sample was finally calcined in a muffle furnace for 4 hrs at 500 ºC and then grinded to a final product of fine powder.

### *2.3 Characterization*

The surface area of the Ni/ZnO catalyst was calculated using N2 adsorption/desorption at 77.4 K using a Surface Area Analyzer NOVA2200e Quanta chrome, USA. A 30 KV Japan scanning electron microscope was utilized to examine the structural morphology of the manufactured Ni/ZnO catalysts. An Oxford Inca EDX, Inca200, was utilized in conjunction with SEM to establish the chemical composition of the produced Ni/ZnO catalyst. Using a JDX3532 JEOL, Japan diffractometer at 40 kV and 30 mA in the 2. XRD investigation was performed on a monochromatic Cu-K radiation (=1. 5418) at 40 kV and 30 mA in the 2 range of 10-800 with 1.030 per minute using a JDX-3532 JEOL, Japan diffractometer.

### *2.4 Application of catalyst for degradation of MY2B and Auramine-O*

For the photo catalytic degradation of MV2B and AO, 50 ppm of working solution was used. For each experiment about 10 mL of the dye solution was taken in a micro reactor and were kept under the UV lamp at fixed distance and intensity in the presence of appropriate amounts of Ni/ZnO catalyst, buffer solution of desired pH and $H_2O_2$ with their varying concentration and/or weight and/or volume. The degradation reactions were carried out using different time interval. After the degradation reaction, the solution was centrifugal at 3000 rpm for 10 min. MV2B and AO degraded dye solution was analyzed using single beam visible spectrophotometer at 586 nm 460 nm respectively against the absorption was recorded.

The absorption of the dye was measure twice one before the degradation and one after the degradation in order to calculate the percent removal with the help of the following formula.

$$\%\,Removal = \frac{C_o - C_f}{C_o} \times 100$$

Whereas, $C_o$ is the initial concentration before degradation and $C_f$ is the final concentration after the degradation.

## 3. Result and discussion

### 3.1 Characterization

### *3.1.1 Scanning 1electron microscopy (SEM)*

**Figure1(a)** demonstrate the result of SEM image of ZnO base. It is evident from the image that undoped ZnO possess a distinct spherical and round shaped morphology with an average size of 229 to 989 nm. From the SEM image of **Figure 1(a)** it can be seen that the undoped ZnO having spherical nano particle without appearance of microsphere. **Figure 1(b)** show the SEM image of Ni-dopped ZnO, which show alternation in the modified sample. It is clearly seen that the morphology of ZnO got alter after Doping with Ni/ZnO. The SEM image of **Figure 1 (b)** illustrate relatively brighter and smaller particle as compared to that of ZnO. As can be seen the particles are aggregated and its sizes are decreases to 88 – 354 nm having high porous surface.

### *3.1.2 EDX analysis of Ni/ZnO*

The catalysts elemental composition for both ZnO and Ni/ZnO was studied using EDX. The spectrum of elements for ZnO is show in **Figure 2 (a),** while for Ni/ZnO catalyst it is shown in **Figure 2(b)**. The EDX spectra shows that nickel is successfully impregnated on ZnO as shown by the **Figure 2(b).** from **Table 1** it is demonstrated that Zn (35.6%) is the most basic and fundamental element while Ni (28.9%), Na (27.8%) and C (21.1%) are the major constituents whereas O (6.2 %) and S (0.30%) are the trace elements on material surface.

### *3.1.3 XRD of Ni/ZnO*

The XRD diffraction patterns of both supports and doped catalysts were taken. In **Figure 2** the chart for both XRD patterns are shown. The diffraction patterns of XRD present all the major peaks for ZnO in **Figure2(a)** while for Ni/ZnO it shown in **Figure 2(b)**. The **Figure 2(a)** present different phases with ICDD numbers 11136, 30888, 361451 and 11244 shows peak at 28°,31°,32°, 34°, 36°, 47°,50°, 56°, 62°, 66°, 67° and 69° and the **Figure 2(b)** for Ni/ZnO and shows pattern according to ICCD number 30888, 30891, 50664, 211486, 471019 and 11025.

## 4. Optimization of different parameters

### *4.1 Effect of weight of catalyst*

It is anticipated that at high concentrations, Ni/ZnO, acting as a solid support, will accumulate a significant amount of methyl violet 2B (MV2B) and auramine O (AO) molecules. In this study, the degradation of MV2B and AO under UV light was assessed using

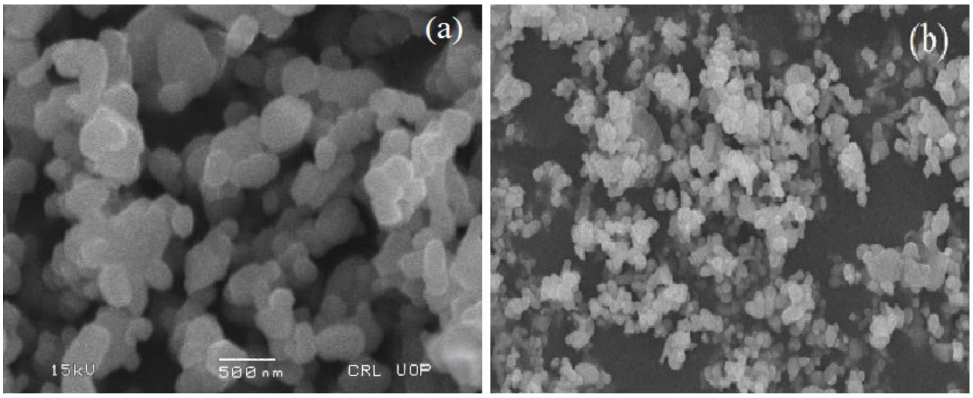


**Figure 1.** SEM images of (a) ZnO and Ni/ZnO

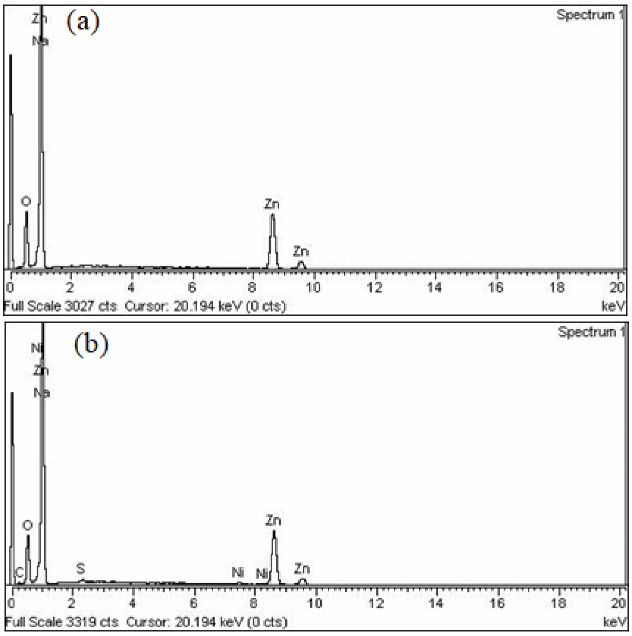


**Figure 2.** EDX analysis of **(a)** ZnO **(b)** Ni/ZnO

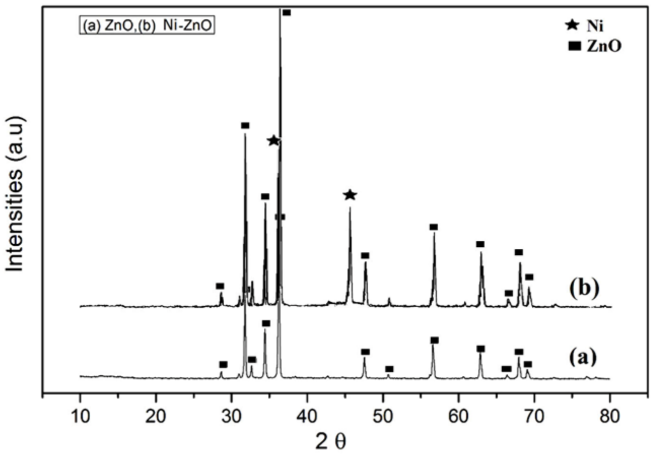


**Figure 3.** XRD graph of **(a)** ZnO and **(b)** Ni/ZnO

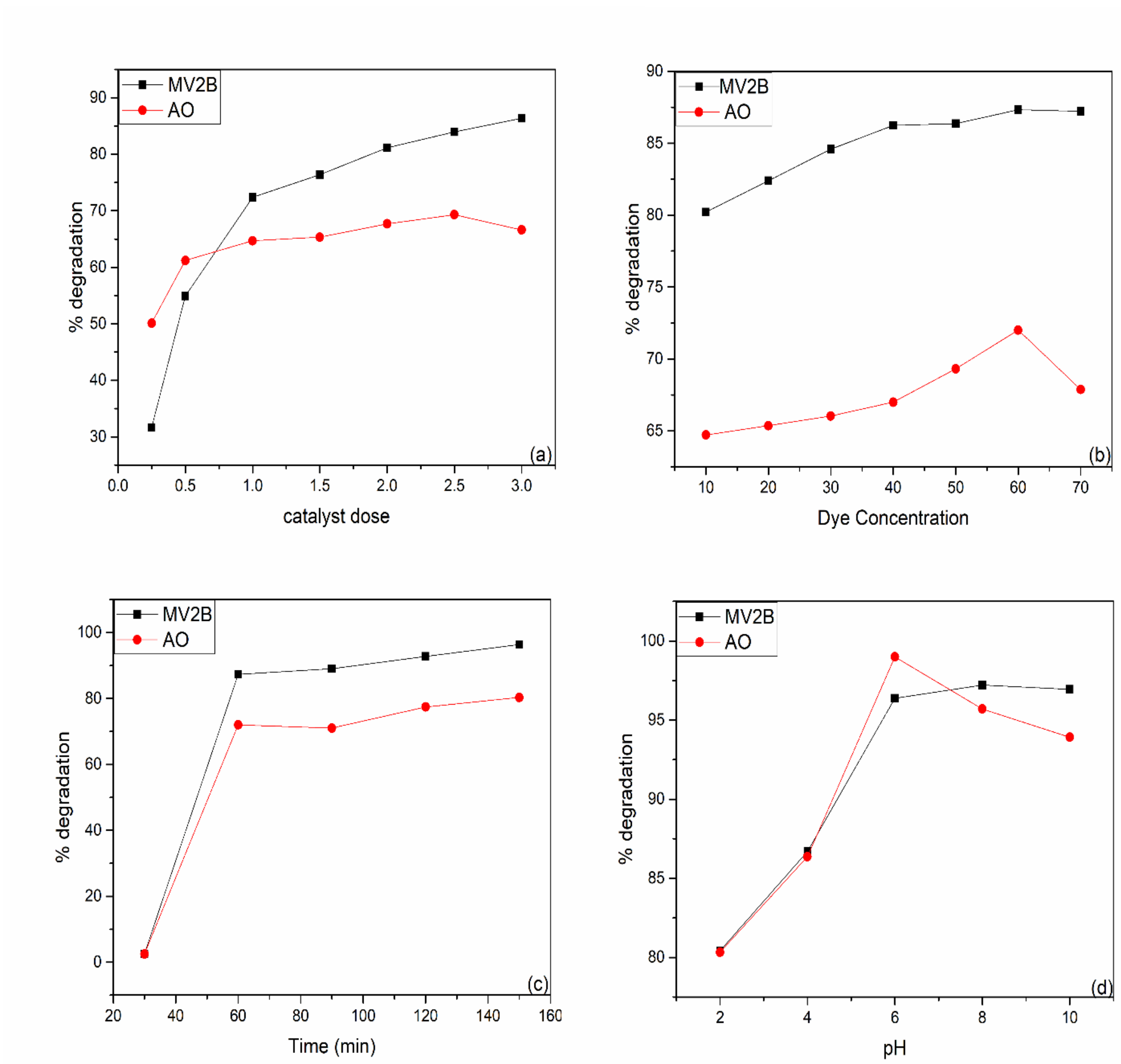


**Figure 4.** **(a)** Effect of catalyst dose **(b)** Effect of initial dye concentration **(c)** Effect of time **(d)** Effect of pH on the degradation of MV2B using 50 ppm dye concentration and, and irradiation time 120 min.

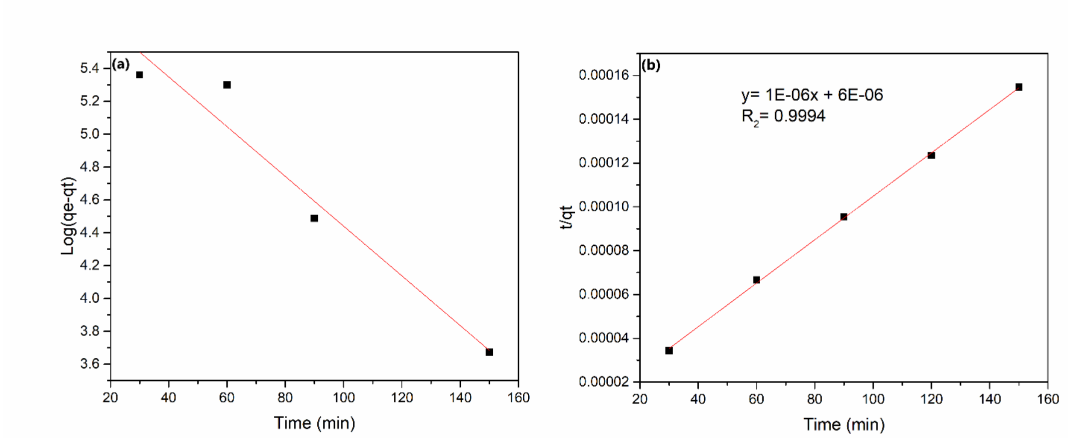


**Figure 5.** **(a)** Pseudo first order kinetic model for AO **(b)** Pseudo second order kinetics model for MV2B with the effect of catalyst weight and time for photocatalytic degradation of AO using Ni/ZnO Photocatalyst.

**Table 1**. EDX composition of ZnO and Ni/ZnO

| Element | Atomic % |
|---|---|
| Zn | 35.6 |
| Ni | 28.9 |
| Na | 27.8 |
| C | 21.1 |
| O | 06.2 |
| S | 0.30 |

**Table 2.** Effect of catalyst Dose on degradation of MV2B and OA

| Catalyst Dose (g/L) | % Removal | |
|---|---|---|
| | MV2B | AO |
| 0.3 | 31.62 | 50.12 |
| 0.5 | 54.92 | 61.21 |
| 1.0 | 72.39 | 64.70 |
| 1.5 | 76.38 | 65.33 |
| 2.0 | 81.15 | 67.69 |
| 2.5 | 83.98 | 69.31 |
| 3.0 | 86.36 | 66.61 |

**Table 3.** Effect of initial dye concentration on degradation of MV2B and AO

| Dye Concentration | %Removal | |
|---|---|---|
| | MV2B | AO |
| **10** | 80.21 | 64.72 |
| **20** | 82.39 | 65.36 |
| **30** | 84.59 | 66.03 |
| **40** | 86.23 | 67.00 |
| **50** | 86.36 | 69.31 |
| **60** | 87.32 | 72.01 |
| **70** | 87.22 | 67.88 |

**Table 4.** Effect of Irradiation time on degradation of MV2B and AO

| Time (min) | MV2B %Removal | AO %Removal |
|---|---|---|
| **30** | 87.32 | 72.01 |
| **60** | 89.03 | 71.01 |
| **90** | 92.79 | 77.43 |
| **120** | 96.37 | 80.33 |
| **150** | 96.37 | 80.33 |

**Table 5.** Effect of pH on degradation of MV2B and AO

| **pH** | **%Removal** | |
|---|---|---|
| | **MV2B** | **AO** |
| 2 | 80.42 | 80.33 |
| 4 | 86.70 | 86.37 |
| 6 | 96.37 | 99.00 |
| 8 | 97.21 | 95.70 |
| 10 | 96.95 | 93.92 |

**Table 6.** Kinetics data for decomposition of Ao and MV2B used Ni/ZnOphotocatalyst

| Kinetic model | Parameters | Values |
|---|---|---|
| | qe (exp) | 990000 |
| **Pseudo first order (AO)** | K1 ($min^{-1}$)<br>$q_e$ calc ($mg\ g^{-1}$)<br>$R^2$<br>C | 0.1529<br>900326.4311<br>0.9499<br>5.9544 |
| **Pseudo second order (MV2B)** | K2 ($min^{-1}$)<br>$q_e$ calc ($mg\ g^{-1}$)<br>$qe^2$ calc ($mg\ g^{-1}$)<br>$R^2$<br>C | 6<br>1000000<br>1E+12<br>0.9994<br>0.000006 |

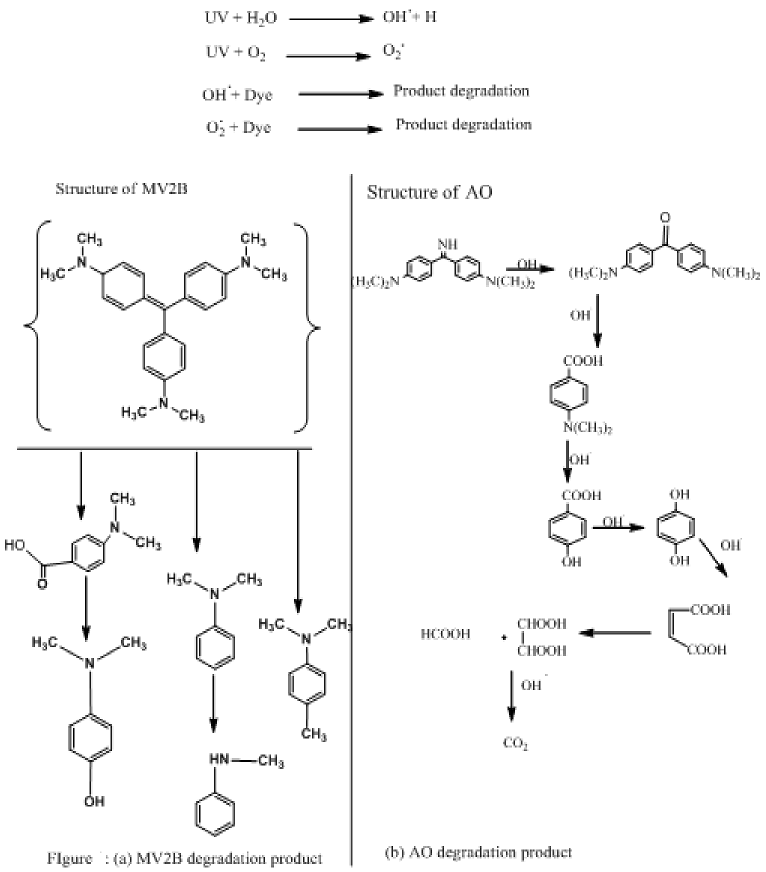


**Figure 6.** (a) Shows the MV2B degradation Product and (b)AO degradation product

various concentrations of the catalyst (0.3, 0.5, 1.0, 1.5, 2.0, 2.5, 3.0 g/L), an initial dye concentration of 50 ppm, and a pH of 6 for a 30-minute irradiation period. The degradation efficiency for each catalyst concentration is presented in Table 2, with maximum efficiencies for MV2B and AO at 86.36% and 69.31% observed at 3 g/L and 2.5 g/L, respectively, as shown in Fig. 3(a). The increase in degradation efficiency with high doses of Ni/ZnO may result from increased adsorption site availability and the driving force for target pollutant accumulation (Iqbal et al., 2019; Nautiyal et al., 2016). Additionally, a high dose of Ni/ZnO is expected to enhance the degradation rate of MV2B and AO due to increased •OH radical formation (Iqbal et al., 2021).

***4.2 Effect of initial dye concentration***

The degradation efficiency of MV2B and AO was also evaluated across a range of initial dye concentrations (10-60 ppm) while keeping other parameters constant (3.0 g/L and 2.5 g/L catalyst for MV2B and AO, 120-minute irradiation time, and pH 6 at room temperature) (Table 3). The findings, shown in Figure 3(b), indicate that degradation efficiency initially increased with dye concentration up to 60 ppm, but further increases led to a decrease due to competition for active sites (Table 4 ) (Nautiyal et al., 2016; Iqbal et al., 2021). Higher pollutant concentrations enhance accumulation and diffusion on the sorbent surface, thus increasing electrostatic and Coulombic attraction forces and thereby raising degradation efficiency (Iqbal et al., 2021; Nasrullah et al., 2018).

***4.3 Effect of time***

The study also investigated the effect of varying UV irradiation times on MV2B and AO degradation, employing 50 ppm dye concentrations, 3.0 g/L and 2.5 g/L Ni/ZnO catalyst for MV2B and AO, respectively, and pH 6, over a time range of 30-150 minutes (Figure 4 (a), (b), (c)). The results showed an increase in degradation efficiency up to 120 minutes, after which the rate plateaued as equilibrium was reached (Table 4). The initial phase (30-120 min) was characterized by rapid degradation due to enhanced interaction between active sites and dye molecules, while the subsequent phase showed a constant rate due to saturation of active sites (Iqbal et al., 2021; Samal et al., 2019).

***4.4 Kinetics studies of MV2B and AO***

The speed of the % photodegradation process and how this speed impacts the equilibrium time are defined using kinetic models. Two kinetic models were investigated: pseudo first order was fitted for AO Eq. 1 and pseudo-second order was fitted for MV2B Eq. 2.

$$\log(q_e - q_t) = \frac{\log q_e - k_1 t}{2.303} \tag{1}$$

$$\frac{t}{q_t} = \frac{1}{q_e} t + \frac{1}{k_2 . q_e^2} \tag{2}$$

Whereas $q_e$ is the removal capacity at equilibrium time (optimum time), $q_t$ is the removal capacity at any time. The optimum time for degradation was 60 min. Where $q_e$ and $q_t$ are the amounts of MV2B and AO degraded photo catalytically (mg/g) at equilibrium and at time t (min). $K_1$ is the rate constant of pseudo-first order process ($min^{-1}$). Linear plot between t (time in min) and log ($q_e$-$q_t$) was used to determine rate constant, qe and qt **Figure 4(a)**. Where the equilibrium degradation ($q_e$) and the second order constant $K_2$ ($min^{-1}$) which linear plot between t/$q_t$ and time to determine $K^2$, qe and qt **Figure 4(b) (c), (d), Figure 5**. The result of the plots investigated that the decomposition of AO follows pseudo first order model of kinetics and the decomposition of MV2B follow second order kinetics because of the closeness of theoretical and experimental values of qe shown in **Table 6.**

***4.5 Effect of pH***

The charge distribution on the surface of the target contaminants and solid adsorbent materials is found to be impacted by changes in pH of aqueous solution (Sayed et al., 2018). For this reason, degradation efficiency of MV2B and AO were investigated by Ni/ZnO by changing pH from 2-10, employing $_0$ = 50 ppm, $[Ni/ZnO]_0$ = 3 and 2.5 g/L for MV2B and AO, for 120 min, respectively, depicted in **Figure 4(d).** It was found that removal efficiency increase with increase in pH from 2 to 8 and maximum degradation were 97.21% and 99% at pH 8 and 6 for MV2B and AO, respectively, as shown in **Table 5.**

**Mechanism of Methyl violet (MV2V) and Auramine-O (AO)**:

The possible photocatalytic degradation of Methyl violet is given below: first the molecules of Methyl violet dye are adsorbed on the surface of the photocatalyst. Which when exposed to UV light the excitation of electron occurs from valence band to the conduction band leaving hole (h+) in the valence band. When electron and holes at the surface of photocatalyst react with dissolved oxygen, adsorbed water molecules and the surfaces hydroxyl groups, so the photo hydroxyl ($OH^•$) and superoxide ($O_2$) radicals are generated. The dye molecules would be degraded by these photo-generated radicals, resulting in intermediates that completely break down into $CO_2$ and $H_2O$ (MV2B). The same Mechanism is for Auramine-O as mentioned above for the MV2B. In the mechanism of Auramine-O there is also the production of ($OH^•$) and superoxide ($O_2$) radicals occurs which are responsible for the degradation of dye.

## 5. Conclusion

The photo degradation experiments were Performed using 257.3 nm UV irradiation. The effects of different parameters such as catalyst weight, Irradiation time, pH have been observed. MV2B degradation without any catalyst was found to be 38.33 percent at 120 min reaction time, while the photo catalyst showed a Substantial improvement in MV2B degradation and a maximum of 92.83 percent with 120 min irradiation time and 300 mg catalyst weight was achieved. The initial pH of the solution was also degraded and the limit was 97.21 percent at pH 8 and the irradiation time was 120 min. The photo degradation experiments were Performed using 257.3 nm UV irradiation. The effects of different parameters such as catalyst weight, Irradiation time, pH and H2O2 concentration have been observed. AO degradation without any catalyst was found to be 67.45 percent in 90 min reaction time, while the photo catalyst showed a substantial improvement in AO degradation and a limit was reached, i.e. 99.58 percent at 90 minutes Ni/ZnO was prepared by wet impregnation method and characterized by surface area analysis (SAA), scanning electron microscopy (SEM), X-ray diffraction (XRD) spectroscopy and energy dispersive x-ray (EDX). The photodegradation studies were carried out using UV irradiation of 257.3 nm. The effect of various parameters like weight of catalyst weight, irradiation time, pH were studied. It was found that the degradation of MV2B without any catalyst was 38.33% in 120 min reaction time, while the photocatalyst showed significant change in the degradation of MV2B and a maximum was achieved i.e., 92.83% with 120 min irradiation time and 300 mg of catalyst weight. The degradation was also effected with the initial pH of the solution and it was maximum 97.21% at pH 5 and irradiation time of 120 min.

## Author contributions

All authors made equal contributions to the study design, statistical analysis, and drafting of the manuscript. The corresponding author, along with the co-authors, reviewed and approved the final version of the article prior to submission to this journal.

## Acknowledgment

The authors were grateful to their department.

## Competing financial interests

The authors have no conflict of interest.

## References

Adegoke, K. A., & Bello, O. S. J. W. r. (2015). Dye sequestration using agricultural wastes as adsorbents. 12, 8-24.

Arabkhani, P., & Asfaram, A. J. (2020). Development of a novel three-dimensional magnetic polymer aerogel as an efficient adsorbent for malachite green removal. Journal of Hazardous Materials, 384, 121394.

Arunagiri, C. (2021). Efficient photocatalytic degradation of organic dyes using $FexZn_{1-x}O$ nanoparticles.

Asfaram, A., et al. (2015). Removal of basic dye Auramine-O by ZnS: Cu nanoparticles loaded on activated carbon: Optimization of parameters using response surface methodology with central composite design. RSC Advances, 5(24), 18438-18450.

Bouasla, C., Samar, M. E.-H., & Ismail, F. J. D. (2010). Degradation of methyl violet 6B dye by the Fenton process. 254(1-3), 35-41.

Chandhru, M., Rani, S. K., & Vasimalai, N. J. (2020). Reductive degradation of toxic six dyes in industrial wastewater using diaminobenzoic acid capped silver nanoparticles. Journal of Environmental Chemical Engineering, 8(5), 104225.

Foroutan, R., et al. (2022). Impact of ZnO and $Fe_3O_4$ magnetic nanoscale on the methyl violet 2B removal efficiency of the activated carbon oak wood. Environmental Technology, 286, 131632.

Ghaedi, M., et al. (2015). Application of ultrasonic radiation for simultaneous removal of auramine O and safranine O by copper sulfide nanoparticles: Experimental design. Ultrasonics Sonochemistry, 136, 1069-1075.

Ghani, I., et al. (2023). Hydrothermal synthesis and characterization of cobalt-doped bismuth oxide NPs for photocatalytic degradation of methyl orange dye. Journal of Alloys and Compounds, 19(7), 1195-1217.

Gul, M., Kashif, M., & Shahid, K. J. (2024). Eco-friendly approaches in the synthesis of ZnO nanoparticles using plant extract: A review. Sustainable Chemistry and Pharmacy, 3(2), 1-25.

Guzmán-Vargas, A., et al. (2016). Adsorption and subsequent partial photodegradation of methyl violet 2B on Cu/Al layered double hydroxides. 363, 372-380.

Hmani, E., et al. (2012). Electrochemical degradation of auramine-O dye at boron-doped diamond and lead dioxide electrodes. Journal of Electroanalytical Chemistry, 30, 1-8.

Hosseinpour, S. A., et al. (2018). Use of metal composite MOF-5-$Ag_2O$-NPs as an adsorbent for the removal of Auramine O dye under ultrasound energy conditions. 32(2), e4007.

Humayun, M., et al. (2016). Enhanced visible-light activities of porous $BiFeO_3$ by coupling with nanocrystalline $TiO_2$ and mechanism. 180, 219-226.

Iqbal, J., et al. (2019). Synergistic effects of activated carbon and nano-zerovalent copper on the performance of hydroxyapatite-alginate beads for the removal of $As^{3+}$ from aqueous solution. Journal of Hazardous Materials, 235, 875-886.

Iqbal, J., et al. (2021). Exploring the potential of nano-zerovalent copper modified biochar for the removal of ciprofloxacin from water. Science of the Total Environment, 16, 100604.

Iqbal, J., et al. (2021). Nano-zerovalent manganese/biochar composite for the adsorptive and oxidative removal of Congo-red dye from aqueous solutions. Science of the Total Environment, 403, 123854.

Jamal, M., et al. (2024). Preparation of manganese-doped bismuth oxide for the photocatalytic degradation of methylene blue. Journal of Catalysis, 1-7.

Jeyasubramanian, K., Hikku, G., & Sharma, R. K. J. W. P. e. (2015). Photo-catalytic degradation of methyl violet dye using zinc oxide nanoparticles prepared by a novel precipitation method and its anti-bacterial activities. 8, 35-44.

Kashif, M., et al. (2023). Bismuth oxide nanoparticle fabrication and characterization for photocatalytic bromophenol blue degradation. Applied Surface Science, 19(07), 521-544.

Kashif, M., et al. (2024). Fe/Ti-codoped strontium oxide nanoparticles for enhanced photocatalytic degradation of methyl orange. Journal of Alloys and Compounds, 11(1), 8-14.

Kashif, M., et al. (2024). Synthesis and characterization of Fe-doped CuO nanoparticles: Catalytic efficiency in crystal violet dye degradation and exploration of electrical properties. Applied Physics A, 3(8), 1-18.

Kommareddi, S., et al. (1984). Nontuberculous mycobacterial infections: Comparison of the fluorescent auramine-O and Ziehl-Neelsen techniques in tissue diagnosis. American Review of Respiratory Disease, 15(11), 1085-1089.

Ma, Y., et al. (2018). Sulfate radical induced degradation of methyl violet azo dye with CuFe layered doubled hydroxide as heterogeneous photoactivator of persulfate. Applied Catalysis B: Environmental, 227, 406-414.

Mosleh, S., et al. (2016). $BiPO_4/Bi_2S_3$-HKUST-1-MOF as a novel blue light-driven photocatalyst for simultaneous degradation of toluidine blue and auramine-O dyes in a new rotating packed bed reactor: Optimization and comparison to a conventional reactor. 6(68), 63667-63680.

Muhammad, P., et al. (2024). Defect engineering in nanocatalysts: From design and synthesis to applications. Catalysis Science & Technology, 2314686.

Nasrullah, A., et al. (2018). High surface area mesoporous activated carbon-alginate beads for efficient removal of methylene blue. Journal of Cleaner Production, 107, 1792-1799.

Nautiyal, P., Subramanian, K., & Dastidar, M. J. (2016). Adsorptive removal of dye using biochar derived from residual algae after in-situ transesterification: Alternate use of waste of biodiesel industry. Journal of Environmental Management, 182, 187-197.

Naz, M., et al. (2021). Elimination of dyes by catalytic reduction in the absence of light: A review. 56(28), 15572-15608.

Nazir, R., et al. (2020). Adsorption of selected azo dyes from an aqueous solution by activated carbon derived from Monotheca buxifolia waste seeds. 15(3), 166-172.

Oguz, E., et al. (2005). Ozonation of aqueous Bomaplex Red CR-L dye in a semi-batch reactor. Dyes and Pigments, 64(2), 101-108.

Qamar, M. A., et al. (2021). Designing of highly active g-C3N4/Ni-ZnO photocatalyst nanocomposite for the disinfection and degradation of the organic dye under sunlight radiations. 614, 126176.

Qi, K., et al. (2020). Design of 2D–2D $NiO/g\text{-}C_3N_4$ heterojunction photocatalysts for degradation of an emerging pollutant. Applied Catalysis B: Environmental, 46, 5281-5295.

Qi, K., et al. (2020). Transition metal doped ZnO nanoparticles with enhanced photocatalytic and antibacterial performances: Experimental and DFT studies. Catalysts, 46(2), 1494-1502.

Reddy, I. N., et al. (2020). Excellent visible-light driven photocatalyst of (Al, Ni) co-doped ZnO structures for organic dye degradation. Catalysis Communications, 340, 277-285.

Sadat, S. A., et al. (2019). Rapid room-temperature synthesis of cadmium zeolitic imidazolate framework nanoparticles based on 1,1′-carbonyldiimidazole as ultra-high-efficiency adsorbent for ultrasound-assisted removal of malachite green dye. 467, 1204-1212.

Safavi, A., & Momeni, S. J. (2012). Highly efficient degradation of azo dyes by palladium/hydroxyapatite/$Fe_3O_4$ nanocatalyst. Journal of Hazardous Materials, 201, 125-131.

Samal, K., et al. (2019). Saponin extracted waste biomass of Sapindus mukorossi for adsorption of methyl violet dye in aqueous system. Environmental Technology & Innovation, 14, 166-174.

Senthil Kumar, M., & Arunagiri, C. J. M. S. M. i. E. (2021). Efficient photocatalytic degradation of organic dyes using Fe-doped ZnO nanoparticles. 32(13), 17925-17935.

Shah, J., et al. (2018). Sonophotocatalytic degradation of textile dyes over Cu impregnated ZnO catalyst in aqueous solution. 116, 149-158.

Shojaei, S., et al. (2021). Application of Taguchi method and response surface methodology into the removal of malachite green and auramine-O by NaX nanozeolites. 11(1), 16054.

Sinha, T., Ahmaruzzaman, M., & Bhattacharjee, A. J. (2014). A simple approach for the synthesis of silver nanoparticles and their application as a catalyst for the photodegradation of methyl violet 6B dye under solar irradiation. Journal of Environmental Chemical Engineering, 2(4), 2269-2279.

SivaKarthik, P., et al. (2017). Comparative study of Co and Ni substituted ZnO nanoparticles: Synthesis, structural, optical, and photocatalytic activity. Journal of Materials Science: Materials in Electronics, 28, 10582-10588.

Sun, Q., et al. (2020). Microwave-induced catalytic degradation of methyl violet by a Ni-$TiO_2$/ACFs composite catalyst. Journal of Hazardous Materials, 277, 128396.

Sun, W., Yao, Y. J. I. J. S., & Technology, T. A. S. (2021). Degradation of auramine-O in aqueous solution by Ti/$PbO_2$-electro-Fenton process by hydrogen peroxide produced in situ. 45(1), 145-154.

Wang, J., et al. (2021). Efficient photocatalytic degradation of methyl violet using two new 3D MOFs directed by different carboxylate spacers. 23(3), 741-747.

Xu, B., et al. (2019). Boosting the visible-light photoactivities of $BiVO_4$ nanoplates by Eu doping and coupling $CeO_x$ nanoparticles for $CO_2$ reduction and organic oxidation. Catalysts, 3(12), 3363-3369.

Xu, K., et al. (2016). Structural and room temperature ferromagnetic properties of Ni doped ZnO nanoparticles via low-temperature hydrothermal method. Journal of Alloys and Compounds, 502, 155-159.

Yan, R., et al. (2022). Comparative study of metal oxides and phosphate modification with different mechanisms over $g\text{-}C_3N_4$ for visible-light photocatalytic degradation of metribuzin. Catalysis Science & Technology, 41, 155-165.

Yang, S., et al. (2013). Photocatalytic degradation of methyl violet with $TiSiW_{12}O_{40}/TiO_2$. Materials Science in Semiconductor Processing, 2013(1), 191340.

Zada, A., et al. (2020). Accelerating photocatalytic hydrogen production and pollutant degradation by functionalizing g-C3N4 with $SnO_2$. 7, 941.

Zada, A., et al. (2021). Review on the hazardous applications and photodegradation mechanisms of chlorophenols over different photocatalysts. Chemosphere, 195, 110742.

Zada, A., et al. (2022). Extended visible light-driven photocatalytic hydrogen generation by electron induction from g-C3N4 nanosheets to ZnO through the proper heterojunction. 236(1), 53-66.

Zaman, S., et al. (2024). Investigating the enhanced photocatalytic degradation of bromophenol blue using Ni/Zn co-doped strontium oxide nanoparticles synthesized via hydrothermal method. Materials Research Bulletin, 3(1), 102-114.

Zhang, Y., Agbaria, R. A., & Warner, I. M. (1997). Complexation studies of water-soluble calixarenes and auramine O dye. Supramolecular Chemistry, 8(4), 309-318.

Zhang, Y., et al. (2012). Ultra-deep desulfurization via reactive adsorption on Ni/ZnO: The effect of ZnO particle size on the adsorption performance. Fuel Processing Technology, 119, 13-19.

Zhang, Z., et al. (2021). Synthesis of Ag-loaded ZnO/BiOCl with high photocatalytic performance for the removal of antibiotic pollutants. Materials Research Express, 11(8), 981.

Zhao, X., et al. (2015). Biochemical synthesis of Ag/AgCl nanoparticles for visible-light-driven photocatalytic removal of colored dyes. 8(5), 2043-2053.

Zhu, J.-H., et al. (2015). Fluorescent carbon dots for auramine O determination and logic gate operation. Sensors and Actuators B: Chemical, 219, 261-267.